Contribution to Volume 54 of *Advances in Atomic, Molecular and Optical Physics.*

Atomic processing of optically carried RF signals

Jean-Louis Le Gouët, Fabien Bretenaker, Ivan Lorgeré

Laboratoire Aimé Cotton, CNRS UPR3321,
bâtiment 505, campus universitaire,
91405 Orsay Cedex, France

Corresponding author email : jean-louis.legouet@lac.u-psud.fr

Abstract : Rare earth ions embedded in crystals are natural high-quality-factor resonators that can be used for processing optically-carried broadband radio-frequency signals. This chapter focuses on the radio-frequency spectrum analysis function and describes different architectures that are designed to reach tens of gigahertz instantaneous bandwidth with sub-megahertz resolution. Various approaches are considered. The active material may act as a spectral buffer memory. Instead one may store a processing function inside the crystal. The latter may then operate either as a frequency-to-angle converter or a frequency-to-time transformer. All those architectures have been explored experimentally. To meet the specific requirements of these processors, frequency agile lasers have been developed. These keynote devices are described in detail.

1. Introduction

When absorbing centers are embedded in a host matrix and the medium is cooled to a few degrees Kelvin, homogeneous absorption line widths are dramatically reduced as a result of strongly diminished environmental fluctuations. While the cooling decreases the homogeneous widths, it has little effect on the inhomogeneous line width that results from the static interaction of the absorbing centers with the host. When exposed to monochromatic

light, the material is excited only within the homogeneous-width of the incoming light and a narrow spectral hole is burned at this position within the absorption profile [1]. This work is part of a long quest for practical applications of spectral hole burning (SHB) in solid materials, an effort that has been pursued since the beginning of the 70's.

The first application considered was optical memory, with the goal of overcoming the storage density diffraction limit by adding a fourth non-spatial dimension, namely frequency, to the memory volume. The initial two patents in this area consider page-oriented storage, where a spatial page of information is stored at a spectral address [2], [3]. To retrieve information one tunes the readout laser to the engraving wavelength. After discovery of permanent SHB in organic materials [4], [5], storage of 2000 [6], 6000 [7] and ultimately 10000 images [8] was demonstrated in chlorine, a porphyrine derivative. A storage density of up to 10Gb/cm² is reached at a temperature of 1.7K by the ETH group [9]. Transfer rate is then limited by the inverse spectral channel width. Time domain encoding of data address can be substituted for spectral addressing [10]. In this approach the Fourier transform of the data sequence is engraved over the inhomogeneously broadened spectral memory absorption band. Then, one has simultaneous access to all the spectral channels. More precisely the data transfer rate equals the inhomogeneous linewidth, a figure that reaches tens of GHz in rare earth ion doped materials such as Tm^{3+}:YAG. This excessively high speed proves difficult to manage and a hybrid chirped carrier technique is proposed. Combining temporal encoding with spectral scan, one has an approach that conveys flexibility to data transfer at both engraving and readout [11] [12] [13]. Despite excellent performance in terms of storage density and capacity, access time and transfer rate, SHB memories suffer from operating at liquid helium temperature, a severe limitation for mass market application.

In the quest of niches for SHB technology, it was soon realized that the specific time/frequency dimension should not be considered on an equal footing with the spatial ones,

as it was in large memory application. Instead, the inhomogeneous linewidth can be regarded as the spectral bandwidth of an optically carried signal analog processor. In this respect SHB materials can outdo any existing electronic processor and appear to be potentially attractive microwave photonics components, offering an instantaneous bandwidth in excess of 10GHz with a channel capacity larger than 10^4.

Application to range and Doppler processing of RADAR return signals has been proposed recently. The cross-correlation function of the encoded RADAR pulse and the return signal is stored as a spectral grating within the SHB material. Even if the pulse encoding is renewed at each transmission, the correlation grating remains unchanged and can be accumulated for milliseconds. Scanning a monochromatic laser through the engraved spectral structure and using a narrow band detector one may retrieve information on target distance and speed with large dynamic range [14]. Another application has been considered for array antennas. For narrow band operation, one directs the gain to the target by adjusting the relative phase shift of the array elements. The phase shift procedure fails to provide an achromatic delay between the array elements in broad band operation, giving rise to the so called “squint effect”. Then “true time delays” can be stored in a SHB material and be applied to arbitrary waveform optically carried signals without latency, either at transmission or reception [15] [16] [17].

Broadband devices are also needed for spectral analysis at the back-end of the heterodyne receivers used in (sub)millimeter astrophysics. The molecular lines observed in astrophysics are generally broadened by either the Doppler effect in the interstellar medium or by pressure in planet atmospheres. In the former case, a 1000km/s-wide spectral window is generally enough to analyze a 700km/s Doppler broadening. If at 100GHz this interval is covered by a 330MHz bandwidth spectrometer, the required bandwidth raises to 10GHz at 3THz, the position of the HD line, and 20GHz at 6THz, the position of the atomic oxygen

narrow line. As for the lines observed in planetary atmospheres, their pressure broadening may reach several GHz and they often exhibit a narrow feature at their center, corresponding to high altitude emission. Both the broad global profile and the narrow central structure usually need be explored. In an heterodyne receiver, the THz range signal, mixed with a local oscillator, is shifted down to the GHz range where its spectral analysis is usually performed either by acousto-optic spectrometers (AOS) or by digital auto-correlators (DAC). The AOS cover a bandwidth of up to 2GHz in a single unit. The DAC offer a smaller bandwidth but their flexible resolution can accommodate fine details such as narrow lines in the dark clouds of our galaxy, with Doppler broadening as small as 0.1-1km/s.

Combining more than 10GHz instantaneous bandwidth with less than 1MHz resolution, SHB materials have the potential to accomplish a breakthrough in RF spectral analysis. In addition they would offer improved power consumption with respect to DAC's together with resolution flexibility and better stability than AOS's. In this paper we review recent experimental achievements that demonstrate SHB capabilities for broadband spectral analysis with a unity probability of intercept. Different approaches have been considered. Some use the SHB material as a storage medium where the optically carried RF signal spectrum is accumulated before readout. Unlike this "spectral photography" scheme, other approaches avoid the storage of the signal under investigation in the SHB medium. Instead the material is programmed as an analog processor that continuously processes the signal-carrying beam. Various programming functions have been explored. Indeed the SHB material is opened to a wealth of wideband spectrum analysis architectures through diverse combinations of space and frequency variables.

After a brief review of conventional RF spectrum analysis techniques in Section 2, we present the spectrum photography architecture in Section 3. Although this is the most recently considered approach it is also the conceptually simplest one. Then we introduce the

programmable filtering approach in section 4, reestablishing the mathematical expression of the SHB material optical response within the framework of a two-level atom ensemble picture. Two demonstrations of analog RF signal processing are then presented in Sections 5 and 6. One processor – the rainbow analyzer – achieves the angular separation of the spectral components while the other one – the photon echo chirp transform analyzer – displays the angular components in the time domain. Keystones of these architectures, specific lasers had to be developed for these experiments. Section 7 is devoted to these devices.

2. Radio frequency spectral analyzers

In this section we review the RF spectrum analyzers that have been considered so far for spatial missions. They have been used at the back end of heterodyne receivers for atmospheric and astronomic observation in the submillimeter and millimeter wavelength range. The THz signal collected by the antenna is mixed with a local oscillator, which shifts its frequency to the GHz range. After amplification the signal is then directed to various RF spectrum analyzers that may include filter banks, acousto-optic analyzers, digital and analog autocorrelators, and surface acoustic wave devices.

In a filter bank analyzer the signal is divided into different spectral channels, each being equipped with its own bandpass filter and detector. Weight and power consumption limits the channel number to a few tens. Bandwidth and resolution are fixed. Missions devoted to solar and atmospheric observation carry those devices [18] [19], each filter bank covering a specific molecular line, with optimum resolution at the line center [20] [21].

Acousto-optic spectral analyzers (AOS) may offer up to 2GHz instantaneous bandwidth in a single compact and low consumption unit. First demonstrated in the 70's [22] [23], these analyzers were used for the first time in a civilian space mission in 1998 [24] [25] [26]. The ODIN satellite [27], launched in 2001, carries an AOS with 1000 channel resolution over 1GHz bandwidth [28]. The forthcoming HERSCHEL mission [29] will also be equipped

with AOS [30] [31] [32]. In an AOS the RF signal to be analyzed is fed to the transducer of an AO modulator. The acoustic wave generates an index grating that diffracts a monochromatic laser beam. The different spectral components of the RF signal give rise to different grating components that diffract the beam in different directions. Diffracted intensity distribution along a photodetector array then reflects the RF signal power spectrum.

Since the Wiener-Khinchin theorem relates the power spectrum to the autocorrelation function, one may record the latter quantity and then retrieve the power spectrum by Fourier transform computation. The quantity to be measured is the time averaged product of the signal and its time delayed replica, at various settings of the time delay. The inverse time delay half size and the number of delay settings respectively determine the analyzer bandwidth and channel number.

In a digital autocorrelator the signal is first processed by an analog to digital converter (ADC). Because of time averaging a poor dynamic range converter can result in excellent dynamic range autocorrelation measurement [33] [34]. Digital processing offers numerous benefits such as stability and absence of additional noise. Delays, supplied by cascaded shift registers, are easily controlled through the clock rate, which gives resolution flexibility. Finally the device is easy to assemble and reproduce [35]. Limitation comes from the sampling rate of the ADC. With a 2GS/s rate (GS/s = Gigasamples/second), available units can offer up to 1GHz bandwidth [36]. Another important limitation is set by power consumption that grows with the bandwidth. ODIN and HERSCHEL missions are equipped with such devices [27] [29] [37] [38].

Increased bandwidth is made available in analog auto-correlators. In these devices two signal replica counter-propagate along two parallel micro-strip lines. The two traveling waves are sampled at taps, evenly spaced along the lines. Different pairs of opposite taps supply different delays between the sampled signals that are subsequently multiplied and digitally

converted [39] [40]. The most advanced system offers an instantaneous bandwidth of 4GHz and 128 channels. Signal attenuation along the microstrips limits the available delay and thus the spectral resolution.

High resolution broadband spectral filtering and large delay generation are tasks that are difficult to achieve with pure electronic means. Hybridizing may help to address these issues as already illustrated by the AOS where optics is combined with electronic processing. Another example of hybridizing is offered by surface acoustic wave (SAW) dispersion lines. By converting the electric signal into a surface acoustic wave one reduces both the wavelength and the delay line dimension in the ratio of sound and light speeds. With the small size acoustic resonant circuits and delay lines that are readily feasible one can build dispersion lines with large group delay dispersion rate. Multiplication by a chirped reference followed by dispersion in the appropriate SAW line performs the signal "*chirp transform*" [41] and results in the desired power spectrum profile [42] [43]. The device to be placed in The Stratospheric Observatory For Infrared Astronomy (SOFIA) will cover 205MHz with 50kHz resolution and 40dB dynamic range [44] [45] [46] [47].

The features of these RF spectrum analyzers are summarized in Table 1.

	Filter bank	Digital Autocorrelator	Analog autocorrelator	SAW	AOS
Bandwidth	1.2GHz	700MHz	3.6GHz	205MHz	1GHz
Channel number	25	100	128	4096	2000
Dynamic range	60dB	48dB	38dB	40dB	30dB
Spectral flexibility	no	yes	no	no	No
Best resolution	NA	140kHz	NA	NA	NA
Interception probability	100%	100%	100%	100%	100%
Access time	FT limited	Integration time	Integration time (>10ms)	FT limited	Readout time

Table 1. Features of current RF spectrum analyzers for sub-millimeter astronomy applications

3. Spectrum photography architecture

3.1. Principle of operation

Although it has been considered only recently [48]-[52]], the spectrum photography architecture is actually the simplest of the three architectures we consider here. It consequently constitutes a good introduction to more complicated schemes which will be discussed later. Its principle of operation can be understood as a two-step process from the scheme of Figure 1.

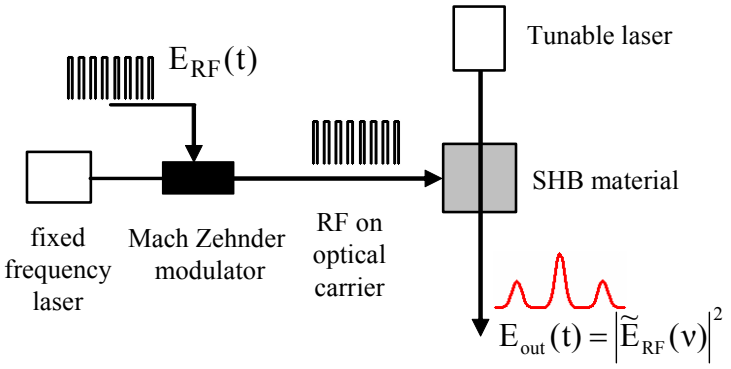

Figure 1. Basic principle of the spectrum photography analyzer.

The RF signal to be analyzed is transposed on a monochromatic fixed frequency laser beam with the help of a Mach-Zehnder modulator. The laser frequency is adjusted in such a way that one of the RF-signal-carrying side-bands lies inside the SHB material absorption band. [see Figure 2(a)]. Upon crossing the SHB material, the beam excites the ions that are resonant with the different optically carried spectral components of the RF signal. Consequently, the optically carried RF spectrum is recorded in the material absorption spectrum [see Figure 2 (b)]. By probing the material transmission with a frequency chirped laser [see Figure 2 (c)] one readily obtains a temporal image of the engraved spectrum [see Figure 2 (d)]. Although the read out scanning procedure is reminiscent of usual electronic spectrum analyzers, the SHB analyzer exhibits a very distinctive feature. Indeed, although spectral addresses are probed sequentially the RF signal is continuously recorded in the SHB material that operates as a spectral buffer

memory. By simply using two separate lasers for engraving and probing one may reach 100 % probability of interception. Storage lifetime in the buffer memory is limited by the excited level population lifetime that can exceed 10ms in the materials we consider. The spectral resolution is limited by the laser noise and the square root of the chirp rate of the reading laser. Given the broad bandwidth to be scanned in less than 10ms, the chirp rate limited resolution will dominate the homogeneous linewidth of the optical transition. The geometry of the experiment can be rather simple, allowing us to consider this experiment as an elementary pixel of a future broadband spectrally resolved RF imaging system.

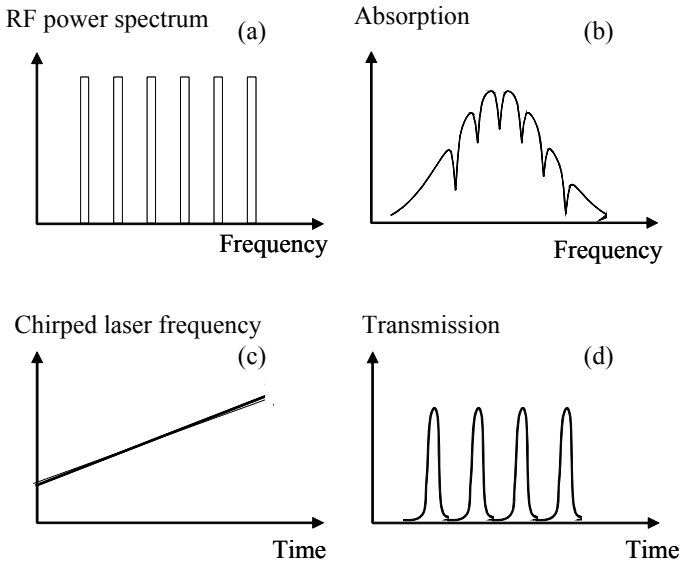

Figure 2. Basic steps of the spectrum photography analyzer. The RF spectrum (a) is engraved in the absorption spectrum (b) which is then read by a frequency-swept laser (c) leading to signal (d).

The principle schematized in Figure 1 has been implemented experimentally. This experiment makes use of a particular type of SHB material, namely a Tm^{3+}:YAG crystal. Before describing this experiment we turn to a short summary of the basic properties of rare earth doped crystals for SHB, with Tm^{3+}:YAG as an illustration.

3.2. Basic spectroscopic properties of Tm^{3+}:YAG for SHB experiments

Rare earth ion-doped crystals (REIDC) represent a satisfactory candidate for high resolution applications. The common structure of rare earth atoms is $5s^2 5p^6 4f^{n+1} 6s^2$, where $0 \leq n \leq 13$. In

triply charged ions, one 4f electron and both 6s electrons are removed. Optical transitions within the $4f^n$ configuration are forbidden for parity reason. Nevertheless some weak lines, with oscillator strength of the order of 10^{-8}, result from mixing with the $4f^{(n-1)}5d$ configuration in sites without inversion symmetry. In addition the sharpness of the lines is preserved, in a solid state matrix, by the shielding of 4f electrons by the 5s and 5p electrons. At 5°K in a crystal host matrix the homogeneous linewidth is usually much smaller than 1MHz. If profitable as far as spectral resolution is concerned, a weak oscillator strength unfortunately means that a larger amount of energy is needed for engraving.

On some transitions the ions behave as two-level atoms, with an excited state that directly decays to the ground state. Then the spectral hole lifetime coincides with that of the excited state. The $^4I_{13/2} \leftrightarrow {}^4I_{15/2}$ transition of Er^{3+} near 1.5μm belongs to this class. It offers a 10ms storage time in the upper level [53]. This material gives access to the wealth of tools that has been developed for fiber-optics communications, including versatile lasers and amplifiers [54].

Different processes may slow down the return to initial state and the spontaneous erasure of the engraved structure. In Eu^{3+} and Pr^{3+} doped crystals, resonant excitation results in an optical pumping alteration of the atom distribution over the ground state hyperfine structure [55]. This alteration may survive for hours before return to thermal equilibrium. The long memory life is obtained at the expense of the bandwidth. Indeed the lines connected to the different hyperfine sublevels overlap, which limits the available bandwidth to a few MHz.

A hyperfine-structure-free-ion, such as Thulium Tm^{3+} is preferred for our broadband processing application. . On the $^3H_4 \leftrightarrow {}^3H_6$ transition in Tm^{3+} doped crystals, a bottleneck metastable state, with a lifetime of about 10ms, delays the excited state decay to the ground state [56] (see Figure 3). The $^3H_4 \leftrightarrow {}^3H_6$ transition wavelength at 793nm is compatible with integrated electro-optic $LiNbO_3$ ultrafast modulators. This wavelength also falls within the range of common semiconductor lasers and of the Titanium-Sapphire laser. Optical pumping

from the ground state to the bottleneck state $^3F_4$ via the upper state $^3H_6$ offers a convenient way to accumulate engraving [57]. Owing to the 500µs lifetime of the upper level, an optical pumping cycle lasts about 1ms. Several cycles can take place during the 10ms lifetime of $^3F_4$. We experimentally verified that a large fraction of the ground state population can actually be transferred to $^3F_4$. This procedure entails two benefits. First optimal engraving can be reached without saturating the $^3H_4 \leftarrow {}^3H_6$ transition, which means lower laser intensity requirements. Second, with a 1kHz refresh rate and a 10ms storage lifetime, the diffraction efficiency is nearly stationary.

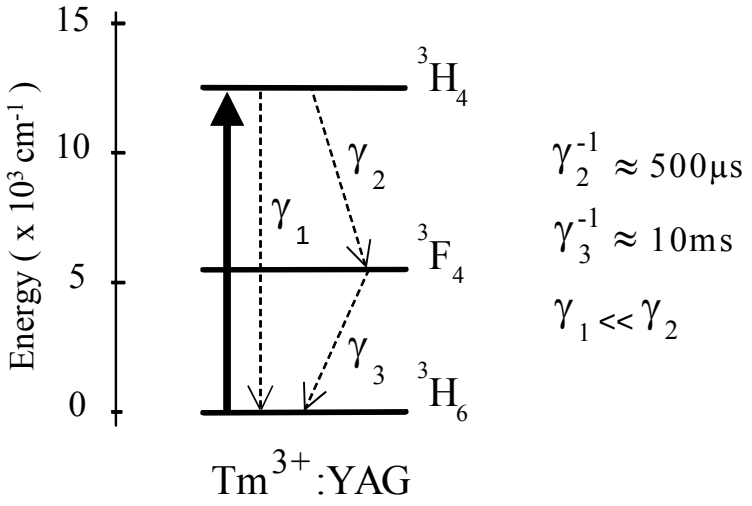

Figure 3. Level scheme in Tm^{3+}: YAG. The laser is coupled to the $^3H_4 \leftrightarrow {}^3H_6$ transition at 793nm. The level decay rates are denoted by γ_i.

3.3. Experimental demonstration

3.3.1. Collinear experiment

The experimental demonstration of the spectrum photography architecture has been first performed using the experiment schematized in Figure 4 [51]. A very similar experiment has been performed at the University of Colorado [52]. The experiment reported in [51] is based on a 2.5-mm long 0.5-at. % doped Tm^{3+}:YAG crystal cooled to 4.5 K. Under these conditions, the peak absorption at 793 nm is 85 %.

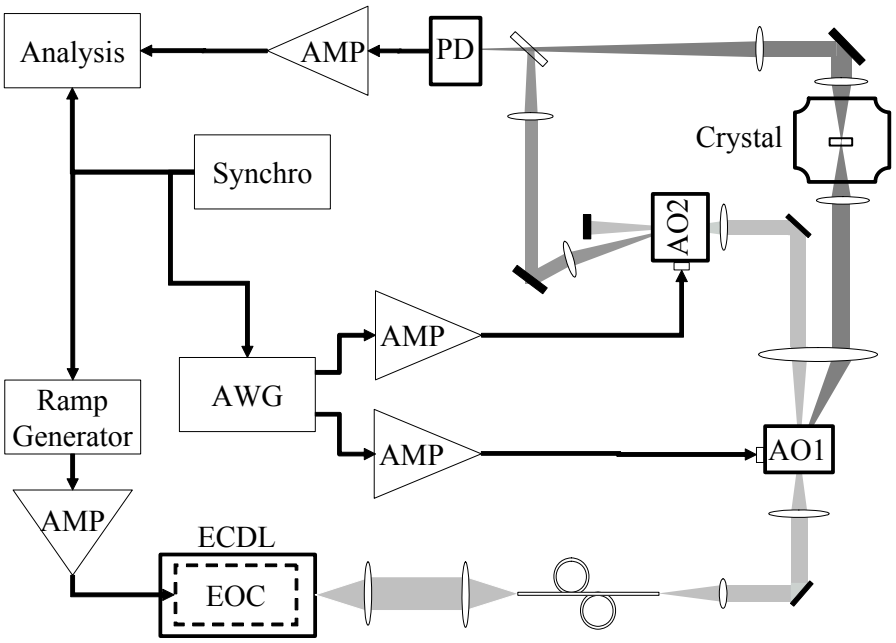

Figure 4. Collinear spectrum photography analysis experiment.

As can be seen in Figure 4, this proof of principle experiment has been performed with only one laser. This laser is a frequency agile external cavity diode laser (ECDL) [58]. It is used alternatively as the engraving laser and as the probe laser of Figure 1. During the engraving stage, the frequency of this laser is tuned by steps to different spectral positions, which mimics an optically carried RF signal. The power of the beam is controlled by the acousto-optic modulator AO1 and is focused to a waist radius w_0 = 90 µm inside the crystal. The zeroth-order beam at the output of AO1 can be frequency shifted using AO1 before being mixed with the beam emerging from the cryostat. This allows performing a heterodyne detection at 5 MHz of the light emitted by the ions, as will be illustrated later. Light is detected using a PIN photodiode (PD) followed by a 10-dB gain amplifier.

An example of a 10-GHz bandwidth spectral analysis is reproduced in Figure 5. The engraved spectrum consists of a series of 16 spikes each lasting 150 µs (pulse energy 450 nJ) with the laser tuned to 16 different frequencies. The reading is performed 1.6 ms later, with a 10-GHz bandwidth scanned in 2 ms. During the reading phase, one reduces the optical power

incident on the crystal to 750 μW, in order not to erase the engraved spectrum. The resulting signal is demodulated and its amplitude is normalized to the unsaturated transmission of the crystal. Among the 16 engraved peaks, 15 are equally spaced by 620 MHz all over the 10-GHz bandwidth [see Figure 5 (a)]. In this experiment, the 16th engraved peak is located 5 MHz apart from one of the 15 equally separated peaks. This doublet is perfectly resolved by our analyzer, as can be seen in Figure 5 (b). The linewidth of each peak corresponds to 2 MHz in this experiment.

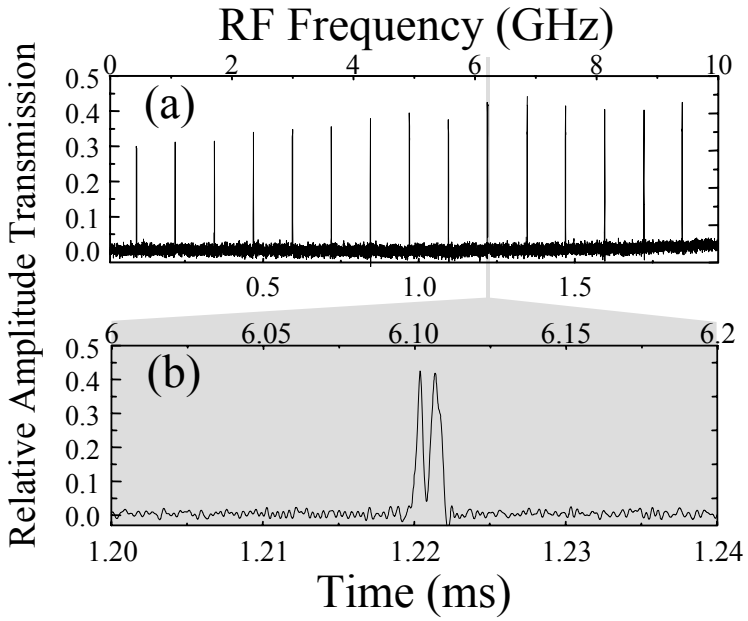

Figure 5. (a) Example of spectrum obtained using the setup of Figure 4. The 10-GHz bandwidth readout is performed in 2 ms. 15 equally spaced tones have been engraved in the sample, except for a 5 MHz doublet, which is perfectly resolved as can be seen in (b).

Of course, this resolution depends on the chirp rate r, as can be seen from the experimental results reproduced in Figure 6. The open circles in Figure 6 represent the measured evolution of the width of a single peak engraved in 200 μs (pulse energy 600 nJ) versus the reading chirp rate. Indeed, it is well known [60] that as soon as the width $\Gamma/2\pi$ of any spectral feature of interest is not much larger than $r^{1/2}$, the readout gets distorted and, in particular, broadened. If we consider a Lorentzian lineshape of width $\Gamma/2\pi$ (in Hz) probed by a light beam of varying detuning $\delta(t) = rt$

(exact resonance occurs at $t = 0$), the resulting time evolution $s(t)$ of the transmitted field amplitude normalized to the undistorted one is given by [61]:

$$s(t) = \mathrm{Im}\left\{ \frac{\Gamma}{\sqrt{r}} \frac{1+i}{2\sqrt{2}} \mathrm{e}^{-\frac{i}{4\pi r}(\Gamma - 2i\pi r t)^2} \mathrm{erfc}\left[\frac{1-i}{2\sqrt{2}} \frac{1}{\sqrt{\pi r}} (\Gamma - 2i\pi r t) \right] \right\}, \quad (1)$$

where erfc stands for the complementary error function. This equation leads to the thick line of Figure 6 obtained with $\Gamma/2\pi = 700$ kHz, which is in very good agreement with the measurements. This value of $\Gamma/2\pi$ is larger than the absolute limit given by twice the homogeneous linewidth of the ions at 4.5 K (2x150 kHz = 300 kHz) because of the contribution of the laser frequency jitter, which will be shown in Section 7.3. This limit linewidth $\Gamma/2\pi$ becomes relevant when it is larger than $r^{1/2}$ whose value is reproduced as a thin line in Figure 6. This shows that a sub-MHz resolution can be reached if the 10 GHz bandwidth is probed in 10 ms, leading to a number of independent frequency bins equal to 10000. Of course, due to the finite lifetime of the engraved spectrum that is limited by the lifetime of the metastable level population (10 ms), the use of a slower chirp in order to improve the frequency resolution and to reach a number of frequency channels equal to 10000 will lead to an increase of the delay before the engraved spectrum is read and hence to a reduction of the detected signal.

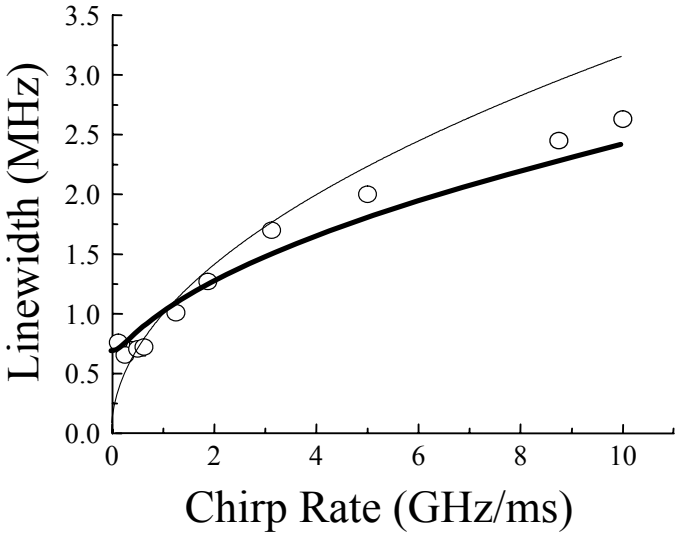

Figure 6. (a) Experimental (circles) and theoretical (thick line) evolutions of the linewidth (full width at half maximum) of a single-frequency readout signal versus chirp rate r. The thin line is $r^{1/2}$.

Another important property of a spectrum analyzer is its dynamic range. It can be extracted from the experimental results reproduced in Figure 7. This figure represents the evolution of single peak readout amplitude versus engraving optical energy. The experimental points have been obtained for two values of the engraving pulse duration (400 µs and 600 µs) and by varying the engraving power. The engraved peak is read after a time delay equal to 1.3 ms. These measurements exhibit a typical saturation behavior, which can be reproduced from a simple three-level rate equation description of the system represented as a full line in Figure 7.

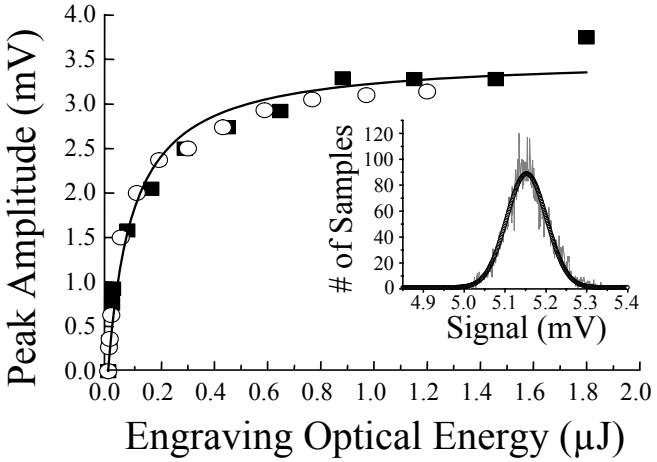

Figure 7. Experimental (circles and squares) and theoretical (full line) evolutions of the detected amplitude of a peak versus the engraving optical energy. The delay between the engraving and the reading of the peak is 1.4 ms. The engraving times are 400 µs (open circles) or 600 µs (filled squares). The theoretical curve is computed with saturation energy equal to 75 nJ. The inset shows the distribution of the signal value in the background absorption region (thin line) together with a Gaussian fit (thick line) leading to a standard deviation of 50 µV.

We estimate the linear part (with a maximum non-linearity of 20 %) of this response to correspond to a signal voltage between 0 and 2 mV. To compare this signal with the typical signal noise, we record 10333 successive samples separated by 8 ns while the laser is chirped in a region where no peak has been engraved. The inset in Figure 7 then reproduces the distribution of the signal value together with a Gaussian fit. The average value of the signal (5.15 mV) corresponds to the transmitted signal when the absorption is not saturated. The standard deviation of this Gaussian noise is found to be equal to 50 µV. The main components of this noise are i) the thermal noise of the detector and amplifier, due to the low value of the detected optical power (a 750 µW incident power is incident on the crystal during the reading stage) and

ii) the low-frequency components of the laser intensity noise. This leads to a value of 16 dB for the linear dynamic range in terms of optical field amplitude of our "photographic scheme" spectral analyzer. Since in this architecture the field emitted by the atoms is directly proportional to the RF signal power, this corresponds to a 16 dB dynamic range for the RF signal also. This relatively poor value is limited by two factors. First, the signal amplitude is rather low, due to the small number of atoms probed by the optical beams. Second, the noise is rather important, due to the fact that our measurements are performed on a non-dark background. Indeed, in this direct transmission experiment, the peaks of Figure 5 are sitting on a background due to the transmitted laser power. The shot noise associated with this background intensity is actually the limiting factor here. This is why we now turn to the realization of a dark background experiment based on a non-collinear geometry.

3.3.2. Non-collinear experiment

The principle of this non-collinear spectrum photography analyzer is summarized in Figure 8, in comparison with the collinear one which has just been described. Figure 8 (a) represents the writing field E_W impinging on the SHB sample in the collinear experiment. During the read-out phase of this experiment [see Figure 8 (b)], the field with real amplitude E_P probes the susceptibility of the material which has been spectrally shaped during the engraving phase. This susceptibility gives rise to a macroscopic polarization that radiates the field E_{RF}, with a real part E_R and an imaginary part E_I. Since the two fields are collinear, the detected intensity is given by

$$I = {E_P}^2 + 2E_P E_R + {E_R}^2 + {E_I}^2 \approx {E_P}^2 + 2E_P E_R \,. \qquad (2)$$

In Eq.(2), the intensity of the RF field emitted by the ions has been neglected because it is usually much smaller than the two other terms. This equation perfectly illustrates the pros and cons of the collinear architecture. Indeed, it shows that the term E_I, i. e., the dispersive response of the atoms, can be neglected thanks to the homodyning or the real part E_R by the probe field amplitude E_P. This leads to the very good frequency resolution of Figure 6. The drawback of this

approach is that the term $E_P{}^2$ is very large and leads to a strong noise which severely limits the signal to noise ratio of the analyzer.

To circumvent this problem, we choose to illuminate the sample with two rather than one engraving beams, as shown in Figure 8 (c). The two engraving beams both carry the same RF signal and are separated by a small angle in the SHB crystal. Consequently, they will engrave a spatial grating only in atoms which are resonant with their spectral components. To read this family of gratings, the chirped probe beam is then incident along the direction of one of the engraving beams, as seen in Figure 8(d). This beam will then be diffracted by the gratings engraved in the spectrum only when it corresponds to an engraved frequency. This is why the RF field E_{RF} emitted by the ions can now be detected on a dark background.

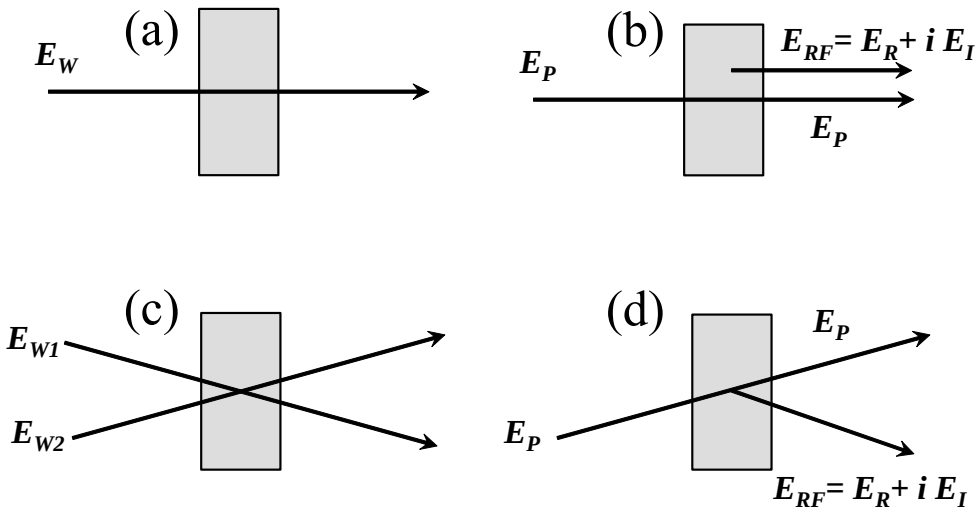

Figure 8. Principle of the (a,b) collinear and (c,d) non-collinear geometries.

The detected intensity is given by

$$I = E_R{}^2 + E_I{}^2 \ . \tag{3}$$

As expected, the probe field intensity and its associated shot noise have disappeared. However, we now have two new problems. First, the detected intensity becomes proportional to the square of the RF power, leading to a decrease of the sensitivity of the analyzer. Second, the system is now sensitive to the imaginary part of the atomic response also. This leads to a strong

degradation of spectral resolution, as illustrated by the experimental result shown in Figure 9 (a). In this figure, one can clearly see that the detection of both quadratures of the emitted field leads to a dispersive-like response of the system. This strongly degrades the spectral resolution of the system. To get rid of the dispersive part of the atomic response, we perform a heterodyne detection of the diffracted beam. To this aim, a fraction of the probe beam is frequency shifted by an acousto-optic modulator operating at frequency *f* and mixed with the diffracted field before it reaches the detector. The detected intensity is given by

$$\begin{aligned} I &= {E_{LO}}^2 + 2E_{LO}E_R\cos(2\pi ft) - 2E_{LO}E_I\sin(2\pi ft) + {E_R}^2 + {E_I}^2 \\ &\approx {E_{LO}}^2 + 2E_{LO}E_R\cos(2\pi ft) - 2E_{LO}E_I\sin(2\pi ft)\ , \end{aligned} \tag{4}$$

where E_{LO} is the local oscillator field amplitude. The detected beat note can be demodulated with the correct phase reference to isolate the term $2E_{LO}E_R$, which contains only the real part E_R of the emitted field. This leads to the experimental result of Figure 9(b). One can see that the dispersive part of the atomic response has been almost perfectly eliminated, in agreement with Eq. (4). According to this equation, one can see that i) the signal intensity is again proportional to the RF signal intensity; ii) the detection no longer occurs on a dark background, due to the presence of the local oscillator intensity. However, the system is now sensitive to the spectral component of the local oscillator intensity noise at frequency *f*, and no longer to the low-frequency part of the intensity noise as in the case of the collinear geometry. A shot-noise limited signal-to-noise ratio is then easier to reach here. Optimization of the signal to noise ratio of the analyzer, i. e. of its linear dynamic range, hence consists in increasing the local oscillator power to increase the signal of Eq. (4), until the total detected power reaches the saturation limit of the detector for the maximum value of the power diffracted by the ions.

Recent results [62], obtained with a 500-µm value for the beam waist inside the crystal, a 10 mW probe beam power, an optimized local oscillator power and a PIN photodiode led to a linear dynamic range approaching 40 dB, together with MHz resolution and 10-GHz bandwidth.

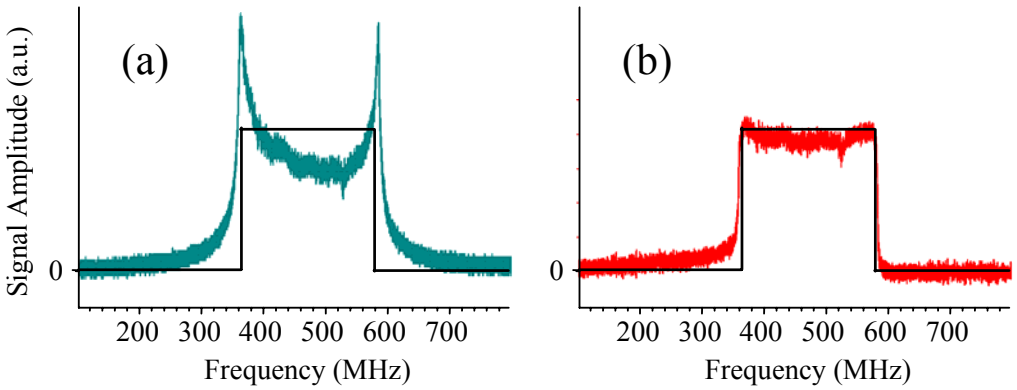

Figure 9. Detected spectrum for the non-collinear experiment. In (a) and (b), the engraved spectrum is represented by the rectangular curve. (a) The total diffracted field is detected. (b) A heterodyne detection permits to isolate the real part of the emitted field and to discard the dispersive part of the atomic response.

Demonstration of the Spatial-Spectral Coherent Holographic Integrating Processor (S^2-CHIP) for analog RF signal processing applications

K. D. Merkel, Z. Cole, R. Krishna Mohan, W. R. Babbitt
Spectrum Lab, Montana State University, Bozeman, Montana 59717
1-406-994-7241 / merkel@spectrum.montana.edu

Abstract

The overall design and an experimental demonstration of the S^2-CHIP, a broadband electro-optic analog signal processor, are presented. The device performs coherent signal processing and integrates multiple correlative acquisition pairs with bandwidths of several GHz and resolves time delays of microseconds with high precision and large dynamic range. High resolution Doppler processing is achievable. Application areas include radar, lidar, and radio astronomy.

1. INTRODUCTION

In a radar range processing system, an optimally encoded RF waveform is transmitted and an antenna receives the scattered target signal that is delayed, attenuated and buried in a noisy background. An analog correlation of the received and reference signals yields the round-trip delay and thus the target's range. Coherent integration of multiple returns increases signal strength and allows for target velocity determination. A spatial spectral (S^2) holographic signal processor has been recently developed as a core-component for a high bandwidth radar-signal processing system [1]. The S^2 material lifetime enables integration of multiple correlative results for range and Doppler processing.

In this paper, we discuss the overall design and preliminary experimental results. These results show the ability to perform range correlation on large data rate (1 Gb/s) biphase-shift-keyed patterns in an S^2 material, Tm:YAG. Results include (1) time delay and range resolution (2) coherent integration of spectral correlations as applied to a radar range processor and (3) dynamic pattern programming.

2. S2-CHIP DESIGN

2.1 Overall concept

The Spatial-spectral Coherent Holographic Integrating Processor, or S^2-CHIP, performs coherent signal processing operations on analog, high bandwidth, and large time bandwidth product optical signals, and integrates the results of multiple acquisitions. Coded RF signals are modulated on a stable optical carrier for processing. A single coherent correlation occurs between two signals in the S^2 material, such as a reference signal and a return signal or, two signals received at different antennas. The S^2-CHIP can determine the delay between these two (or more) signals, while at the same time analyzing Doppler shifts introduced from target movement. The integration of multiple correlation signals relies on the short-term persistence of the S^2 material.

The practicality of the device comes from the fact that the input signals being processed can be of very high bandwidth, while the resultant output signal is low bandwidth. This eliminates the optical-to-electronic bottleneck in the overall device performance.

2.2 Applications / Insertion point

The S^2-CHIP is a coherent integrating processor that could be inserted into several systems requiring high performance evaluation of signals. These include:

Active Radar
- Single-element or large multi-element phased arrays
- Range, mid to high Pulsed Doppler
- Detecting and locating stealth communications
  - Including frequency hopping radio

Radio Astronomy Signal Processing
- Analyzing radio astronomy signals
- Search for Extra-Terrestrial Intelligence

LIDAR and Laser Radar:
- Atmospheric monitoring / wind shear measurements
- Space-based tracking of satellites or other targets

2.3 Design and operation

The device has a stabilized external cavity diode laser (ECDL) as a source for generating a cw optical carrier on which to transmit information. The cw carrier is modulated to create optical pulses to carry the RF modulation of the radar to the crystal. The modulation from the RF domain to the optical domain is achieved by electro-optic phase modulators that change the optical carrier phase in proportion to the sign and magnitude of the applied RF voltage. One modulator is used for the reference waveform, and another one for the received signal from the radar. The S^2 crystal responds to the power spectrum of the optical inputs and stores a S^2 grating. This grating contains the information about the target in terms of the amplitude, frequency and phase variations. The grating is the result of multiple series of optical inputs.

A chirp EOM is used for reading out the S^2 grating. This modulator frequency scans the cw carrier slowly over the stored grating, where it experiences frequency dependent absorption, thereby mapping the programmed spectral features. The output signal is detected by a high sensitivity photoreceiver. This low bandwidth optical to electrical conversion generates a low bandwidth analog electrical signal that is digitized with an high performance low bandwidth A/D converter and rendered digitally for post-processing and analysis.

For range Doppler processing, the key idea is to combine aspects of spatial multiplexing to create a bank of parallel filtering operations. In each spatial location, Doppler processing would occur with a shifted carrier frequency for the reference waveform, where accumulation occurs when the carrier and Doppler shift match. In short, the spatial spatial location with the strongest accumulation signal would represent the frequency closest to that experienced by a Doppler shift. An array of dectectors and A/D converters is used.

2.4 Components

2.4.1 Frequency stabilization of external cavity diode lasers

Laser stability is an important consideration, since the system performs coherent processing and the phase stability of the optical carrier could limit the system performance. Research groups at MSU have pioneered frequency stabilization of cw ECDLs to narrow, transient spectral holes as frequency references burned in an S^2 material. [2] ECDLs have been stabilized to 20 Hz precision at 793 nm using Tm:YAG – an achievement of 2 parts in 10^{13}. These levels of stabilization are more than sufficient for a successful implementation of a commercial S^2-CHIP.

2.4.2 Electro-optic modulators E/O and RF electronics

The telecommunications industry has made available high quality components for optical transmission windows through optical fibers at 800 nm, 1300 nm, and 1550 nm, and the associated electronics to drive these systems. These electro-optic modulators and electronics are commercially available off-the-shelf components, with typically specified properties that are ideally suited for use in an S^2-CHIP. Both digital and analog RF driving electronics up to 12 Gb/s are available.

2.4.3 Broadband optical amplifiers

Amplification of broadband phase and/or amplitude modulated optical signals is required for parallel processing. While erbium doped fiber amplifiers are commercially available at 1550 nm, there is no such widely commercially available amplifier system at 793 nm due to a lack of leverage in the marketplace. There are 3 present options for amplification, 1. Injection locking, 2. Semiconductor optical amplifiers, and 3. Raman fiber amplifiers. Research groups at MSU have developed amplification using injection locking of a high power diode laser near 800 nm up to 6 Gb/s [3]. Injection locking is being used in our demonstrations, but other options are being investigated.

2.4.4 S^2 materials

Collaboration between Spectrum Lab, MSU Physics Department and Scientific Materials Corporation has led to the growth, characterization and utilization of high quality S^2 materials. Material parameters of specific interest include, inhomogeneous linewidth (sets system bandwidth), oscillator strength (sets bandwidth and power consumption), material coherence time (sets coherent processing duration), grating lifetime (sets integration time), crystal orientations (determines efficiency), and spectral diffusion (can reduce performance). While materials can be designed and further optimized for future applications, currently available materials can be used to make practical devices. The two material systems of greatest interest for the proposed work are Tm:YAG (0.1 at. %, 793 nm transition) and Er:YSO (0.001 at. %, 1536 nm transition), each offering a 10 ms integration time, and 30 GHz of bandwidth.

2.4.5 Cryocoolers

The S^2-CHIP system requires a compact cryocooler at 5K with a low level of vibration on the 10 Hz time scale. Reliable, turn-key, maintenance-free, closed cycle cryocoolers are currently commercially available for 0.5 W operation at 3.6K and 1.0 W at 5K. A watt of cooling power would handle multiple (~1000) beams in one material sample. The PT4-5 pulse tube cyrocooler available from Cryomech Corp. offer the best combination of specifications, with vibration levels at 20 mm on the 1.4 Hz time scale. The PT405 will be used in the next S^2-CHIP demonstrator. Efforts continue to dampen small vibrations, and sub-3 μm displacement is possible. Present day cryocooler efficiency is currently 10 kW/W (10 kW wall power per 1 watt cooling power). When compared to the power drawn by comparable parallel digital processing systems, this cryo-power penalty becomes insignificant. In the next five years, the market for 4 K cryocoolers is expected to push performance higher while reducing cost due to their use in new magnetic resonance imaging units. A forecast from cryogenic experts for 2008 is that a 1.0 W at 4K pulse tube cryocooler will sell for half the current cost ($20k vs $40k) with twice the efficiency, a more compact design, less vibration, and higher reliability.

2.4.6 Frequency swept laser pulses

The S^2-CHIP system will utilize a frequency swept laser pulse to readout the grating, which can be created with an electro-optic element either external or internal to the laser cavity. Either of these methods could be used and are being presently explored.

2.4.7 Photoreceivers and A/D converters

The readout process leverages the enormous performance and cost advantage of using low bandwidth photoreceivers and analog-to-digital converters. A photoreceiver would need only a 1 MHz bandwidth and, near 800 nm using a Si photoreceiver cell and transimpedance amplifier, the dynamic range could exceed 90 dB. Current off the shelf analog-to-digital converters at 2.5 MS/s have specified 16-bit quantization performance. Such devices enable the full use of the processing material's dynamic range.

2.5 S^2-CHIP device features

The device using a currently available S^2 material, Tm:YAG, offers analog signal processing applications the following:

- Large signal processing bandwidths (30 GHz)
- Large time bandwidth product signals (>1000)
- Analog waveform processing
- Large dynamic range
- Pulse repetition frequencies from ~1 kHz – 1 MHz
- Coherent integration over 10 ms, up to 1000 shots
- Doppler shift resolution of ~ 100 Hz
- Agile coding ability (transmitted waveform changes from shot to shot)
- Reconfigurability on the ~ms timescale

3. THEORY FOR EXPERIMENT

The present demonstration was done in context of a radar range correlator. Future work will focus on high PRF Doppler processing in a similar context. To summarize, in radar range and Doppler processing applications, a pulse sequence is transmitted and the received signal is delayed, attenuated, and buried in noise after being reflected by a target. Correlation between the return and transmitted signals yields the round-trip time of flight as a delay τ. When the reference and return signals are modulated onto the same optical carrier, an S^2 processor records their spectral interference with a modulation period $1/\tau$. The S^2

material's persistence time allows for coherent integration of multiple acquisitions. Integration of N coherent correlations increases the intensity of the correlation peak by N^2, while the noise grows as N. The integration time also provides resolution for frequency analysis of return signals to determine Doppler shifts from a moving target according to its velocity.

Readout was performed with a low power transmitted chirp pulse which experiences frequency dependent absorption. The resultant signal is detected, A/D converted, and post-processed to extract delay information. The chirp rate should be less than $(1/\tau_m)^2$ where τ_m is the maximum resolvable delay, in order to ensure sufficient spectral resolution. For example, if the chirp rate is 1.0 MHz / μs, then for 1 GHz grating bandwidth the latency is 1.0 ms, and the required detection bandwidth is 1 MHz.

For the experimental demonstration, each programming shot consisted of an M-bit bi-phase shift keyed (BPSK) waveform (i.e. radar reference signal) and a single time delayed replica (i.e. radar return signal), where a unique pulse pair n = 1, 2, …N was introduced at the pulse repetition frequency (PRF). The delay is fixed for all shots. Dynamic coding was performed, where each programming shot contains a unique, zero-mean BPSK waveform and its time delayed replica. Using dynamic codes in coherent integration enhances the primary frequency component while the other spectral features (e.g., temporal sidelobes) change each shot.

4. EXPERIMENTAL RESULTS

4.1 Summary

Results on (1) time delay and resolution (2) coherent integration of spectral correlations and (3) dynamic pattern programming are presented. An optical beam stabilized to sub-10 kHz over 10 ms by locking to a transient spectral hole in Tm:YAG [2], was electro-optically encoded and amplified with injection locking [3] before irradiating the S^2 material. This demonstrator system has been assembled and utilizes existing technology and materials.

4.2 Experimental setup

Figure 1 shows the main components of the experimental setup. A cw Ti:Sapphire laser was centered at 793.380 nm and frequency stabilized to a transient spectral hole in one spatial location of a 4 mm long Tm:YAG (0.1 at. %) sample at 5.0 K. The stabilized laser was split into two beams for processing and readout. The processing beam was modulated by an electro-optic phase modulator (EOM) driven by a pulse pattern generator. The light was continuously BPSK modulated, such that each pattern was modulated at 1 Gb/s and between any patterns the light was square wave (…101010…) modulated at 1 Gb/s. After modulation, the processing beam was amplified by injection locking a high powered slave diode laser. The readout beam was modulated by an acousto-optic modulator (AOM) driven by an arbitrary waveform generator to create a linear frequency chirped pulse around a 265 MHz carrier. A cube was used to combine the beams, which were focused to a ~50 μm spot in the sample. The beams were then incident on a 125 MHz photodetector.

For all experiments, the processing waveforms were 512 bits (512 ns) BPSK sequences and the PRF was 100 kHz. The processing beam power was 2.5 mW. The readout beam power was 100 μW and chirped over ~40 MHz at a rate sufficient to resolve the longest time delay. Higher readout bandwidths will give larger dynamic range.

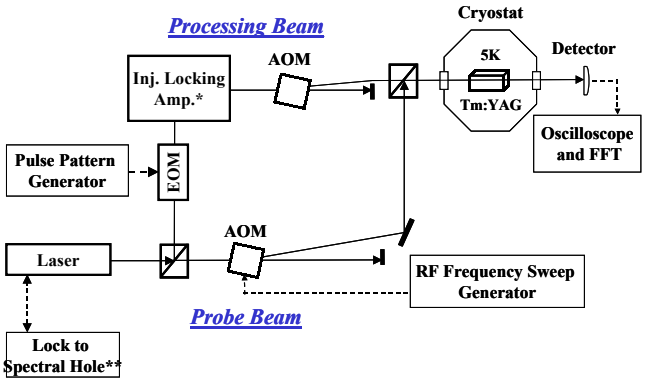

Figure 1 Depiction of basic demonstrator system used. * Injection locking optical amplifier; **Frequency locking the laser linewidth to a transient regenerated spectral hole, technologies developed at MSU.

4.3 Results

Figure 2 shows the results of processed time delay profiles ranging from 0.6 - 1.0 μs that were extracted from the power spectrum of transmitted readout signal. Plotted is the log magnitude squared of the Fast Fourier Transform of the data. The peak widths depend on the readout bandwidth and the peak signal decreases with increasing time delay due to finite material coherence time. Under these conditions, dynamic range >40 dB and range jitter <1 ns were observed. Higher temporal resolution and dynamic range is expected at higher readout bandwidths.

For coherent radar returns, integrated signal processing leads to signal enhancement and noise averaging. Figure 3 plots the calculated RMS values for the peak strength versus the number of programming shots (log-log scale), with a fixed delay (1 μs) with four different powers in the processing beam, each varying in factors of 2. The processing powers were 2.5 mW, 1.25 mW, 0.625 mW and 0.3125 mW. Each data set shows that the

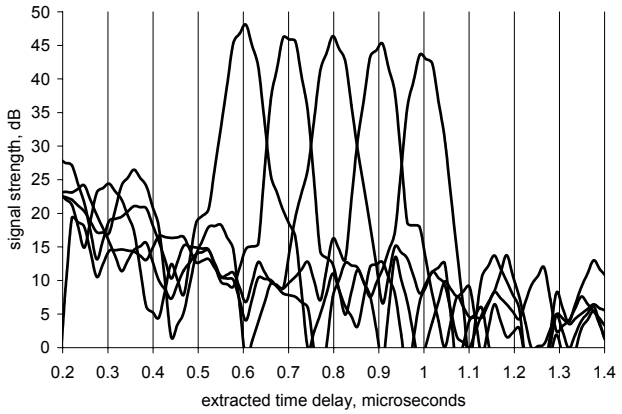

Figure 2 Time delay over 0.6-1.0 μs, showing 40 dB dynamic range. The processing sequences were repeated for 200 shots at 100 kHz, where each shot consisted a unique dynamic 512 bit pattern with 1 Gb/s BPSK modulation and its delayed replica.

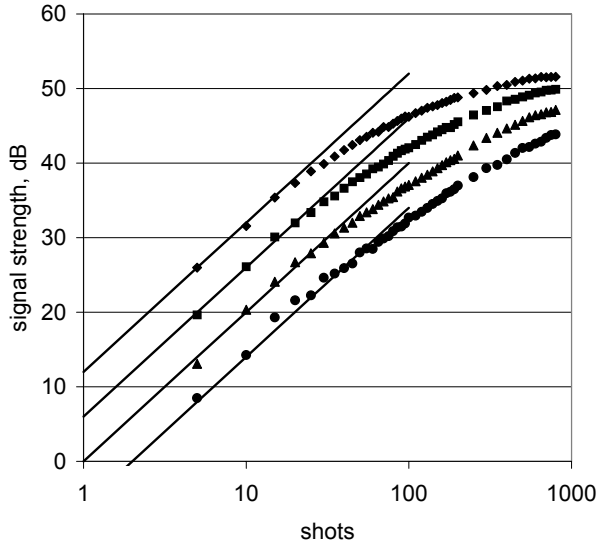

Figure 3. Accumulation dynamics rms peak signal strength versus N programming shots for 2.5 mW programming power (top curve) and decreasing factors of 2 in power versus ideal coherent accumulation N^2 (solid lines).

processed signal strength initially grows ideally as the square of the number of shots, as expected, but then exhibits power dependent roll-off due to saturation before reaching a steady state. In general, for lower power more shots can be ideally coherently integrated. For 0.3125 mW, the satuation point is roughly 85 shots, while for 2.5 mW it is roughly 15 shots. When the power was raised to 5 mW (not shown here) the integration varied, indicating coherent saturation of the individual processing shots.

Dynamic or agile coding is a desirable feature for advanced radar systems. Figure 4 shows the evolution of the signal and side-lobe strengths for agile and single pattern programming. The signal growth for both is nearly identical. But, while the fixed side lobes of single pattern grow with the signal, the varying side-lobes of dynamic patterns average out. An enhancement ~25 dB in the dynamic range under these conditions was achieved by using dynamic coding at 800 shots.

The performance of these preliminary demonstrations begin to show the necessary bandwidth, frequency resolution, integration time and dynamic range required for modern high performance radars. Further increases in processing and readout bandwidths are being implemented along with range-Doppler processing.

5. SUMMARY

In summary, coherent signal processing and integration of up to 800 dynamically changing shots was demonstrated. The processing data rate was 1 Gb/s. The demonstration used an Tm doped YAG crystal held at 5.0K, a frequency stabilized continuous wave laser, commercially available telecom components, and a low-power chirped pulse probe. Time delays of 0.6 to 1.0 μs were programmed and extracted. We believe that the techniques introduced here represent substantial progress

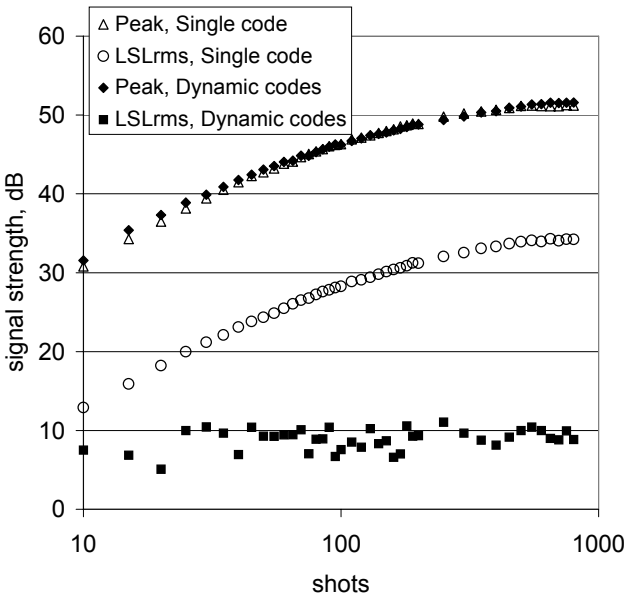

Figure 4. The effect of agile processing with dynamic patterns is shown. The 'Peak' and the calculated rms left sidelobe 'LSLrms' values are plotted for both agile programming with dynamic patterns and accumulation with fixed pattern.

towards a practical, high performance, multi-GHz, analog coherent integrating temporal processor.

6. ACKNOWLEDGEMENTS

Our thanks to NASA Ames Research center with support under grant NAG2-1323, and to Scientific Materials Corp, Bozeman, MT, Kelvin Wagner, University of Colorado, Boulder, for conceptual contributions and support for this work.

7. REFERENCES

[1] Z. Cole, T. Böttger, R. Krishna Mohan, R. Reibel, W. R. Babbitt, R. L. Cone and K. D. Merkel, Appl. Phys. Lett. 81, 3525 (2002)

[2] N. M. Strickland, P. B. Sellin, Y. Sun, J. L. Carlsten, and R. L. Cone , Phys. Rev. B 62, 1473 (2000)

[3] R. R. Reibel, Z. W. Barber, M. Tian, W. R. Babbitt, Z. Cole, K. D. Merkel, J. Opt. Soc. Am. B 19 2315 (2002)

8. BIBLIOGRAPHIES

All of the authors presently work at the Spectrum Lab of Montana State University. Kris Merkel received his Ph.D. in Electrical Engineering from the University of Washington in 1998. R. Krishna Mohan received his Ph.D. in Optical Physics in 1994 from the Indian Institute of Science. Zack Cole received his M.S. in Physics in 1999 from Montana State University. Wm. Randall Babbitt is the director of the Spectrum Lab and a professor of Physics at Montana State University. He received his Ph.D. in Physics from Harvard University in 1987. All are members of the Optical Society of America.